

A population of faint, old, and massive quiescent galaxies at $3 < z < 4$ revealed by JWST NIRSpec Spectroscopy

Themiya Nanayakkara^{1*}, Karl Glazebrook¹, Colin
Jacobs¹, Lalitwadee Kawinwanichakij¹, Corentin
Schreiber², Gabriel Brammer³, James Esdaile¹, Glenn G.
Kacprzak¹, Ivo Labbe¹, Claudia Lagos^{3,9,10}, Danilo
Marchesini⁴, Z. Cemile Marsan⁵, Pascal A. Oesch^{3,6}, Casey
Papovich⁷, Rhea-Silvia Remus and Kim-Vy H. Tran^{8,9}

^{1*}Centre for Astrophysics and Supercomputing, Swinburne
University of Technology, P.O. Box 218, Hawthorn, 3122, VIC,
Australia.

²IBEX Innovations, Sedgefield, Stockton-on-Tees, TS21 3FF,
United Kingdom.

³Cosmic DAWN Center, Niels Bohr Institute, University of
Copenhagen, Jagtvej 128, Copenhagen N, DK-2200, Denmark.

⁴Physics and Astronomy Department, Tufts University, 574
Boston Avenue, Medford, MA, 02155, USA.

⁵Department of Physics and Astronomy, York University, 4700
Keele Street, Toronto, ON, M3J 1P3, Canada.

⁶Department of Astronomy, University of Geneva, Chemin Pegasi
51, Versoix, CH-1290, Switzerland.

⁷Department of Physics and Astronomy, and George P. and
Cynthia Woods Mitchell Institute for Fundamental Physics and
Astronomy, Texas A&M University, College Station, TX
77843-4242, USA .

⁸School of Physics, University of New South Wales, Kensington,
Australia.

⁹ARC Centre for Excellence in All-Sky Astrophysics in 3D.

¹⁰International Centre for Radio Astronomy Research, University
of Western Australia, 7 Fairway, Crawley, 6009, WA, Australia.

¹¹Universitäts-Sternwarte, Fakultät für Physik,
Ludwig-Maximilians-Universität München, Scheinerstr. 1, 81679,
München, Germany.

*Corresponding author(s). E-mail(s): wnanayakkara@swin.edu.au;

The confirmation of the presence of very massive quiescent galaxies at epochs only 1–2 Gyr after the Big Bang [1–8] has challenged models of cosmology and galaxy formation [9]. Producing sufficient numbers of these requires abundant numbers of the host dark matter halos to have been assembled and sufficient time for star formation to proceed extremely quickly and then cease just as rapidly. Ground-based spectroscopy has suggested ages of 200–300 Myr [3] at redshifts $3 < z < 4$. The true number and ages of these objects have however been highly uncertain as ground-based spectra has been limited to the brightest of them [e.g. 3, 5], at wavelengths $\sim 2\mu\text{m}$, which introduces a significant potential bias towards younger objects [7]. The launch of the James Webb Space Telescope (JWST) enables dramatically more sensitive and constraining spectroscopic observations due to the very low sky background, sharp image quality, and access to wavelengths beyond $2\mu\text{m}$. Here we report JWST NIR-Spec [10] (0.6–5.3 μm) observations of 5 new quiescent galaxy candidates that were beyond the limit of previous ground-based spectroscopy. The high signal/noise spectra of galaxies with continuum significantly fainter than earlier confirmations show that they are also at redshifts $3 < z < 4$, and that they have substantial stellar masses of $\sim 0.5 - 1.0 \times 10^{11} M_{\odot}$ comparable to massive galaxies in the nearby Universe. One of the galaxies has been quenched for $\gtrsim 1$ billion years pointing to a presence of substantially older and fainter galaxies than those revealed so far by ground-based spectroscopy. This suggests that some of the massive galaxies have very early formation epochs (during the epoch of reionization, $z \gtrsim 6$, [e.g. 11]) pointing to a need for high conversion rates of baryons to stars in the first massive galaxy halos in the early Universe [12, 13].

We present the detection of 5 new quiescent galaxies at $z \approx 3 - 4$ with spectra obtained by the JWST. Our objects were selected from the sample of Schreiber+2018 [henceforth S18 14] whom compiled a deep complete spectroscopic analysis of massive quiescent galaxy candidates at $z > 3$ obtained using rest-frame $U - V$ vs $V - J$ color selection techniques with pre-JWST data [15]. The prior ground-based spectra covered wavelengths 1.5–2.3 μm and were taken with the MOSFIRE spectrograph on the 10m Keck telescope [16] with up to 14 hours on-target exposures. Out of the 24 massive galaxy candidates observed, spectroscopic redshifts were obtained for only 12 of the galaxies. However, the majority of these objects were found to have redshifts $z > 3$, where only two were low-redshift interlopers. The $z > 3$ galaxies were all

typically brighter than $K = 23$, as the observations are limited by the bright terrestrial K -band background. This potentially introduces a significant age bias. At these redshifts the observed K -band probes the rest frame B -band. At fixed mass younger objects will have smaller B -band mass-to-light ratios and hence be brighter. Conversely, older objects, which could form earlier and hence be more constraining on theoretical models would be dominated by older stellar populations with higher mass-to-light ratios (and therefore would be fainter) [7].

On 1st of Aug, 2022 using JWST NIRSpec we obtained spectra of five massive quiescent galaxy candidates from S18 that had eluded ground-based spectroscopic confirmation. Additionally, due to close clustering we were able to include ZF-8197, a galaxy that was confirmed by S18 in one of our configurable microshutter array (MSA) configurations [17]. Our observations used the MSA to form programmable slits and the low-resolution ($50 < R < 500$) prism disperser with the CLEAR filter covering wavelengths $0.6 - 5.3 \mu\text{m}$. Here we present results from two MSA configurations (`obs100` and `obs200`)¹ observed over the ZFOURGE UDS field [18]. We used 5 slitlet shutters with 3 dither positions. Each dither position was observed for 657s. The data were reduced using the publicly available pipeline `rwst v1.10.0` with JWST Calibration Reference Data System (CRDS) context `rwst_1089.pmap` provided by STScI [19]. In Figure 1 we show the 2D raw and reduced frames of one of our MSA configurations, `obs100`. Three primary targets fall in this mask and the continua of these objects are clearly visible in the ramp-fitted raw frames.

The absolute flux calibration accuracy of data reduced with post launch calibration files is expected to be at $\lesssim 5\%$ level (STScI, private communication). However, the pipeline currently does not account for slit loss functions accurately for NIRSpec MOS extended sources. Therefore we used multi-band NIRC*am* imaging from the PRIMER survey to apply an empirical scaling to the data as follows. For each object, we selected all photometric bands within $1.0 \mu\text{m} - 5.0 \mu\text{m}$ detected with a S/N of > 20 and computed the offset between the flux measured from the NIRSpec spectrum and broadband/medium-band photometry. We then fit a 2nd order polynomial to the offset as a function of wavelength to obtain a spectrophotometric scaling factor for each galaxy. The order of the polynomial was chosen carefully via visual inspection for each object, to verify no artificial structure or colour term would be introduced to the spectra as a result of this process. We multiplied the observed spectra by this calibration function to obtain NIRSpec spectra which are consistent with the PRIMER photometric data. More details on the scaling process and associated tests performed to verify the calibration accuracy of the STScI pipeline are provided in the Methods Section 2.1.

In Figures 2 and 3 we show the calibrated NIRSpec spectra for our galaxies observed over the ZFOURGE UDS field. All six galaxies show a strong Balmer break confirming their post-starburst nature. The Balmer and D4000 break

¹We select these two configurations due to overlap with JWST PRIMER-UDS imaging (G)-1837 PI Dunlop), which is crucial for spectrophotometric calibrations.

of a galaxy is indicative of the nature of stellar populations dominating the continuum [e.g. 20]. Once the young O stars move off the main sequence, the galaxy continuum is dominated by late-B and main sequence A stars which gives rise to a Balmer break. The strength of this feature will reduce after a few hundred million years from the most recent star-formation episode due to A type stars moving away from the main sequence. Thus, at older ages, absorption from ionized metals from old late type stars' atmospheres will dominate the absorption features at $\sim 4000\text{\AA}$. In the early Universe, due to the limited lifetime for galaxy evolution, Balmer break galaxies will dominate over D4000 break galaxies. JWST NIRSpec/Prism observations are expected to uncover large populations of Balmer break galaxies in the early Universe [e.g. 21].

Two of our galaxies, ZF-8197 and ZF-3651 show prominent emission lines. Based on their [O III] $\lambda 5007$ /H β flux ratios, we cannot rule out Active Galactic Nuclei powering the emission lines of these galaxies [22]. The continua of all galaxies are detected at a median S/N of > 10 . While the resolution of NIRSpec Prism observations is too low to constrain detailed element abundant patterns through absorption lines, we can clearly see spectral signatures of H β and H γ in absorption. Dusty interlopers can contaminate photometric selection of quiescent galaxies [23], however, with our NIRSpec Prism observations we can confirm that none of our photometrically selected galaxies are $z \sim 2$ dusty interlopers.

In Figure 2 we also show the ground based Keck/MOSFIRE [24] spectra obtained for two of the galaxies to compare with our new JWST observations. The native resolution of MOSFIRE is $R \sim 3000$. S18 binned the spectra to ~ 10 resolution elements to increase the continuum S/N. Given our NIRSpec/Prism observations have a much lower resolution of $R \lesssim 100$ at $\lambda_{obs} \sim 2\mu m$ (where the Balmer break falls), we rebin the MOSFIRE spectra to 250\AA bins to accurately compare with our NIRSpec observations.

ZF-8197 has strong [O III] $\lambda 4959\lambda 5007$ doublet detection that falls within the MOSFIRE- K band. Thus, S18 obtained a confident redshift confirmation with an on-source exposure time of $\sim 7h$ reaching an emission line S/N of ~ 12 . Even though MOSFIRE observations reached a continuum S/N of ~ 16 with 70\AA spectral binning, it was not possible to obtain signatures of absorption lines. Given the Balmer break largely falls within the atmospheric cutoff between H and K bands, it was not possible to confirm the post-starburst nature of this galaxy. However, with our new NIRSpec observations we are able to observe the Balmer break and other strong emission lines such as H α and [S II] $\lambda 6717\lambda 6731$.

ZF-7329 was observed for $\sim 10h$ in K -band with MOSFIRE reaching a continuum S/N of ~ 17 . However, S18 was unable to obtain a spectroscopic redshift confirmation for this source due to the limited wavelength coverage. Our NIRSpec observations show the clear spectral shape of this object and our `slinefit`² redshift estimate puts it at $z = 3.207$. The Balmer break of this galaxy is smoother compared to our other five galaxies and the spectral features

²<https://github.com/cschreib/slinefit>

have transitioned to a D4000 break suggesting a much older underlying stellar population [25]. However, degeneracies between dust and SFH can make the interpretation difficult. Thus, we use FAST++ [3] to perform full spectral fitting of our galaxies to constrain their SFHs.

We simultaneously fit PRIMER NIRC*am* photometry with JWST/NIRSpec spectra together in FAST++ keeping redshifts fixed at their new spectroscopic values. We use BC03 [26] stellar population models with a Chabrier [27] IMF and follow a Calzetti [28] dust prescription model. We allow the metallicity to vary between 20% to 100% Z_{\odot} . We mask out strong emission lines in the observed spectra and follow the same prescription as defined by S18 to parameterize the SFHs. To account for the low and non-linear spectral resolution and dispersion of the NIRSpec PRISM mode observations, we compute empirical line spread functions (LSF) for our galaxies based on the PRIMER NIRC*am* images. As outlined in [11, Section 2.3], for each galaxy we compute the 1D slit profile across each of the 7 PRIMER NIRC*am* bands and multiply with the PRISM dispersion function to obtain a measure of the LSF. This profile is input into FAST++ as the SPEC_LSF_FILE option, which is used by FAST++ to convolve the BC03 models to match with the observed NIRSpec resolution. The errors of all parameters are computed as the $1-\sigma$ distribution of the best-fit values of 100 Monte-Carlo iterations. More details of the spectrophotometric fitting process is outlined in methods Section 2.2 and in [11]. The FAST++ best-fit results are presented in Table 1.

Our galaxies show relatively low levels of SFR and the stellar masses range between $\sim 0.4 - 1.1 \times 10^{11} M_{\odot}$. This can be compared with a characteristic stellar mass of $\sim 0.5 \times 10^{11} M_{\odot}$ expected at $z \sim 3$ [29]. It is evident that all of our galaxies are massive ($> 10^{10} M_{\odot}$) with relatively low levels of SFR. Half of our galaxies have relatively low levels of dust attenuation ($A_v \lesssim 0.4$). ZF-7542 shows the highest amount of dust at $A_v = 1.4$ suggesting a non-negligible amount of dust in some of these early massive systems. In Figures 2 and 3 we also show the best-fit (lowest- χ^2) spectrum for our galaxies. All galaxies are well constrained by the parameters used in our fitting. We have extensively worked with the data reduction to constrain wiggles in the observed spectra and determine features that are not well reproduced by stellar populations models. This is further detailed in [11] and a full analysis of the our GO-2565 sample will be presented in Nanayakkara et al. (in prep) once the wider COSMOS-WEB Cycle 1 GO program is concluded.

Before JWST/NIRSpec was available, the limited spectral coverage from ground based spectroscopy and uncertain redshifts purely based on photometric data made it challenging to constrain the formation timescales. With spectroscopy we are able to obtain a redshift measurement and to accurately constrain the shape of the SEDs for galaxies without a very sharp Balmer break, (i.e., the more evolved objects). Furthermore, we are able to quantify any emission line contamination to the photometry (which can produce larger rest-frame optical breaks than the stellar continuum) which could result in

an overestimate of the stellar masses. Therefore, with joint spectrophotometric fitting with FAST++ we are able to tightly constrain galaxy formation and quenching timescales.

Figure 4 shows the reconstructed SFHs based on FAST++ best fitting results. To be consistent with [11], we have trimmed the spectra of ZF-7329 at rest-frame $\sim 0.7\mu\text{m}$ in FAST++ fitting. At the redshift of observation ZF-7542 is the youngest galaxy in our sample reaching 50% of the stellar mass only in the last ~ 200 million years. At the opposite end ZF-7329 reached its 50% of the stellar mass ~ 1.8 billion years before it is observed redshift of $z \sim 3.2$. While all galaxies classify as quenched based on the S18 definition, it is clear that there is a large variety in quenching time scales. ZF-8197 has only reached the $0.1 \times \langle SFR \rangle_{\text{main}}$ quenching definition very recently in the last 100 million years, while ZF-7329 has been quenched for $\gtrsim 1\text{Gyr}$. Once rest $U - V$ and $V - J$ colors are recomputed for our sample at their spectroscopic redshifts with strong emission line contributions removed [23], we find that all galaxies lie inside or near the border of the quiescent region. ZF-8197 was previously observed in S18 and was ruled out as a star-forming galaxy based on rest $U - V$ and $V - J$ colors, however with newer constraints from JWST, we find that it falls at the boundary between star-forming and quiescent.

Are such high numbers of massive quiescent galaxies plausible at $z \sim 3 - 4$? As shown by several studies (e.g 30–32) current cosmological simulations find it challenging to reproduce observed number densities of massive quiescent galaxies at $z > 3$. With our current observing program we have targeted sources selected in the pre-JWST era which eluded ground based spectroscopic confirmations. Our joint spectrophotometric analysis has confirmed that our five new galaxies also fall within the quenched definition used by S18.

S18 reported 20 $z \sim 3 - 4$ massive quiescent galaxies in the full ZFOURGE field. This was based on an accuracy of 80% (5/24 galaxies were reported as non-quiescent) for non-spectroscopically confirmed candidates. We spectroscopically confirm five more galaxies, thus, we compute that full ZFOURGE field should hold 21 $z \sim 3 - 4$ massive quiescent galaxies leading to a number density of $\sim 1.5 \times 10^{-5} \text{Mpc}^{-3}$ (ZF-8197 only reached the quiescent definition in the $\lesssim 100$ Myrs, so to be conservative, we don't consider ZF-8197 to be quiescent in this analysis). This can be compared with $0.6 - 3.6 \times 10^{-5} \text{Mpc}^{-3}$ obtained respectively at $z = 3.7$ and $z = 3$ with Illustris-TNG 100 [8]. SHARK simulations also find a similar number density evolution for quiescent galaxies at $z \sim 3 - 4$ [31]. Additionally, at $z \sim 4$, the local environment of galaxies has also shown to play a role in determining the quiescence of galaxies [13].

If our current success rate of photometric selection of massive quiescent systems holds for the rest of our program, the end of our program will provide tighter constraints to the abundance and formation epochs of massive quiescent galaxies in the early Universe that can be robustly compared to simulations as it will then form a complete K -band selected sample. The statistics will enable to provide tighter constraints to galaxy formation and mass buildup mechanisms at $z > 6$, going beyond what has been possible in the pre-JWST era

[e.g., 7, 33, 34]. Additionally, early results from JWST Early Release Science imaging have shown evidence for more massive quiescent galaxy candidates at $z > 3$ [35] that were not selected by ground-based surveys. If these sources are also spectroscopically confirmed, our understanding of galaxy evolution in the early Universe will need to shift.

On average, recent simulations are able to reproduce currently observed number densities of quiescent galaxies up to $z \sim 3$ [8, 31, 32], and depending on environment even up to $z = 4$ [13]. However, details such as ages are still in tension and under investigation from several simulation approaches. In order to reconcile observed number densities of massive quiescent galaxies at $z \sim 3 - 4$, simulations require either a revision of how supermassive black hole feedback regulate galaxy growth and star-formation quenching in galaxies in the first 1 – 2 billion years of the Universe, or a revision of gas/dust depletion timescales and star burst properties of the early Universe. As many simulations currently investigate possible impacts of modified Active Galactic Nucleus (AGN) feedback (e.g., Illustris-TNG, SHARKS & EAGLE, private communication), but also different depletion timescales and star formation models [e.g., 36, the Magneticum Pathfinder Team, private communication] on the star formation and quenched properties of high redshift galaxies, observations such as those presented here will be critical to refining our understanding of the complex balance of physical processes that play the key role in the early epochs of galaxy formation.

Prominent broad [OIII] λ 5007 and H α emission lines are visible in two of our galaxies which could be indicative of AGN activity. The [OIII] λ 5007/H β diagnostic from [22] suggests that these emission lines could be powered by an AGN. Given the low resolution of the PRISM mode observations, we are unable to separate the broad and narrow components of these emission lines. Thus, we cannot rule out secondary contribution from star-formation to these lines. Recent results have shown evidence for AGN to play a prominent role in the evolution of massive quiescent galaxies at $z \sim 3 - 5$. For example, NIRSPEC medium resolution spectroscopy of a $z \sim 4.6$ quiescent galaxy candidate [37] show clear evidence for broad outflows likely driven by an AGN. Similarly, the most massive galaxies spectroscopically confirmed at higher redshifts also allude to presence of accreting black holes [38]. In our sample, most of the younger quiescent galaxies do show strong emission line ratios consistent with powered through AGN activity. While the post-starburst nature of low mass galaxies at $z > 5$ [39, 40] could be driven by the prominence of strong star-bursts, our massive galaxies would likely require more intense feedback mechanisms to shut down star-formation. Future work needs to explore the role of AGN feedback vs intense star-formation within the context of the new generation of large cosmological simulations to test efficient quenching mechanisms of early massive galaxies [e.g. 41]

Our understanding of the formation of these early quiescent systems will improve rapidly due to the new capabilities of JWST. The new data presented here are only 33 minute integrations of *HST* selected samples at relatively low

spectral resolution with a median S/N of $\sim 10 - 40$ and are only a first look. Future higher spectral and spatial resolution JWST/NIRSpec observations of these galaxies have the capability to strengthen our understanding of the stellar populations, initial mass functions [42], and mass buildup mechanisms and timescales through measurements of their kinematic properties and abundance measurements of multiple elements [43]. These massive quiescent galaxies provide a fossil record of star-formation in the Universe prior to $z = 4$, in systems where nature has helpfully formed an abundance of stars in one place where detailed high signal/noise spectral analysis with JWST will be possible.

This work is currently limited to presenting a first JWST/NIRSpec view of a *HST* selected population of massive quiescent galaxy candidates. The work mirrors the approach taken by S18 to provide a view of the transformative capabilities of *JWST*. A thorough analysis of ZF-7329 is presented in [11] with advanced modelling of parametric and non-parametric star-formation histories. Morphological analysis based on $1 - 5\mu\text{m}$ PRIMER imaging of our galaxies rule out any secondary reddened components for our sources (e.g. [44, 45]). A detailed JWST/NIRcam morphological analysis of the S18 sources will be presented by Kawinwanichakij et al. (in prep). Nanayakkara et al. (in prep) will present the full S18 sample observed by GO-2565 program upon completion of data acquisition and analysis with complex star-formation modelling including detailed contributions from AGN using BEAGLE [46] and Prospector [47].

1 Figures and Tables

2 Methods

2.1 Spectrophotometric Calibration

The galaxy data analyzed in this study was processed using the STScI NIRSpec pipeline, with stages 1, 2, and 3 executed under the CRDS context `jwst_1089.pmap`. The end products of this pipeline are 2D rectified, background-subtracted, and wavelength- and flux-calibrated spectral images, as well as a box car extraction from the 2D product.

A significant limitation of the existing JWST/NIRSpec pipeline arises from the computation of the light `pathloss` function, which accounts for light loss due to the Multi-Shutter Assembly's (MSA) finite slit size (geometrical losses including those due to the PSF width) and the light dispersion stemming from the instrument's finite pupil size (diffraction loss) [49]. The JWST flight calibration uses observations of slit-centred standard stars whose reference spectrum is known. Thus centred point sources receive an empirical absolute spectrophotometric calibration accounting for these geometric and diffraction losses.

For more complex sources the pipeline uses a theoretical optical model [49] to calculate the relative pathloss compared to a centred point source. However the pipeline only has models for non-centred point sources and for sources that uniformly fill a slit. Considering that our galaxy sample primarily consists of

Table 1 Galaxy spectroscopic redshifts, NIRC*am* F_{200W} band magnitudes, and FAST++ best fit parameters for galaxies presented in this analysis. FAST++ parameters are as defined as in S18. 1σ upper and lower bounds for FAST++ measured values derived using 100 MCMC iterations included with the best fit parameters.

Galaxy ID	z_{spec}	F_{200W} mag	M_* $\log_{10}(M_{\odot})$	A_V mag	SFR_{10} $\log_{10}(M_{\odot}/yr)$	t_{quench} $\log_{10}(yr)$	t_{form} $\log_{10}(yr)$	t_{SF} $\log_{10}(yr)$	$\langle SFR \rangle_{main}$ $\log_{10}(M_{\odot}/yr)$
3651	3.796 ^{+0.003} _{-0.003}	23.48 ^{+0.23} _{-0.48}	10.55 ^{+0.56} _{-10.55}	1.0 ^{+0.98} _{-0.92}	-4.24 ^{+4.24} _{-4.58}	8.17 ^{+8.2} _{-8.17}	8.27 ^{+8.28} _{-8.27}	7.67 ^{+7.67} _{-7.52}	2.88 ^{+3.03} _{-2.88}
4347	3.712 ^{+0.003} _{-0.003}	23.67 ^{+0.23} _{-0.67}	10.44 ^{+0.44} _{-10.44}	0.4 ^{+0.38} _{-0.32}	-15.63 ^{+15.63} _{-15.63}	8.57 ^{+8.57} _{-8.57}	8.6 ^{+8.6} _{-8.6}	7.36 ^{+7.36} _{-7.36}	3.1 ^{+3.1} _{-3.1}
6496	3.973 ^{+0.003} _{-0.003}	23.14 ^{+0.23} _{-0.14}	10.87 ^{+0.87} _{-10.87}	0.0 ^{+0.0} _{-0.0}	-0.37 ^{+0.37} _{-0.37}	8.11 ^{+8.11} _{-8.11}	9.0 ^{+9.0} _{-9.0}	9.07 ^{+9.07} _{-9.07}	1.85 ^{+1.85} _{-1.85}
7329	3.207 ^{+0.003} _{-0.003}	22.86 ^{+0.22} _{-0.86}	11.09 ^{+11.05} _{-11.05}	0.1 ^{+0.16} _{-0.03}	-2.42 ^{+2.42} _{-2.42}	9.08 ^{+9.08} _{-9.08}	9.25 ^{+9.25} _{-9.25}	8.49 ^{+8.49} _{-8.49}	2.67 ^{+3.19} _{-2.65}
7542	3.200 ^{+0.003} _{-0.003}	23.43 ^{+0.23} _{-0.43}	10.64 ^{+0.64} _{-10.64}	1.4 ^{+1.45} _{-1.32}	-3.87 ^{+3.83} _{-5.67}	8.18 ^{+8.18} _{-8.18}	8.24 ^{+8.24} _{-8.24}	8.28 ^{+8.28} _{-8.28}	2.36 ^{+3.56} _{-2.35}
8197	3.545 ^{+0.003} _{-0.003}	23.87 ^{+0.23} _{-0.87}	10.37 ^{+0.37} _{-10.35}	0.9 ^{+0.88} _{-0.82}	-1.86 ^{+1.86} _{-2.79}	7.89 ^{+7.89} _{-7.89}	8.43 ^{+8.43} _{-8.38}	8.14 ^{+8.14} _{-8.14}	2.24 ^{+2.85} _{-2.24}

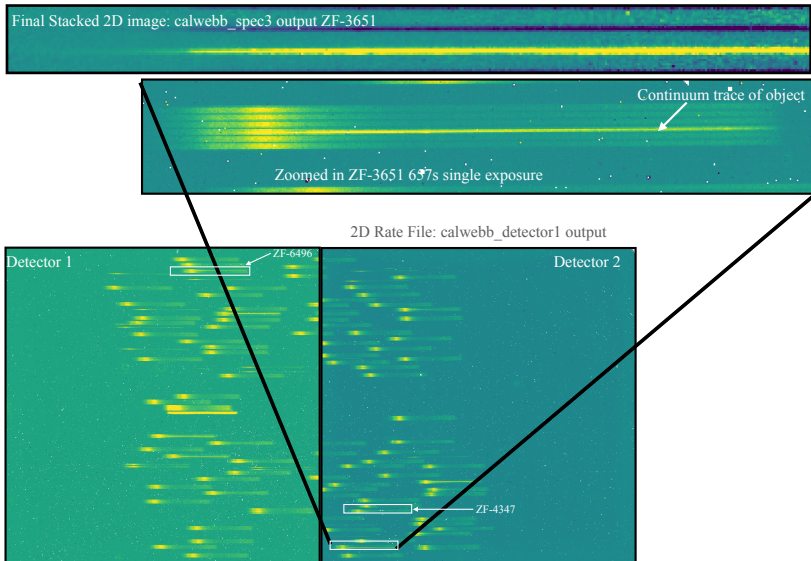


Fig. 1 An example of raw and reduced data obtained by our program. The lower panels show the first exposure of our ZFOURGE UDS mask `obs100`. The data has been processed through the `calwebb_detector1` pipeline which has combined the raw frames of the exposure (ramp fitted). This was a 657s exposure (similar to all exposures carried out by our program) and three of our quiescent candidates: ZF-4347, ZF-3651, and ZF-6496 were covered by this pointing. We have highlighted the positions of these three galaxies in the detector using white boxes. The continuum traces from our $z > 3$ galaxies can be clearly seen in this exposure. In the middle panel we have zoomed into the region in the detector which covers ZF-3651. The continuum of the object and the bar shadows from the MSA can be seen clearly. The upper panel shows the final reduced 2D image of ZF-3651. Three exposures of 657s in three dither positions have been combined to produce the positive trace of this object which is optimally extracted and shown in Figure 3.

compact galaxies (Kawinwanichakij et al., in prep), neither scenario accurately represents their morphology. Estimating a correction based solely on morphological parameters is complicated and necessitates a model that accounts for the spatial light distribution of the object as a function of wavelength, including PSF effects.

Our first goal is to empirically verify that the absolute spectrophotometry *through the slit*, including PSF effects, is accurate. Our logic is that JWST NIRC*am* images should have a very similar PSF to that seen by NIRSpec as to first order the PSF represents the telescope optics diffraction with the different backend instrument optics creating only secondary modifications. Therefore we can add pseudo-slit apertures to NIRC*am* images and compare fluxes in these apertures to the NIRSpec spectra. We use the NIRC*am* PRIMER images³ and superimpose artificial slits in a 5-slit pattern over 3 dither positions on the reduced PRIMER images (Kawinwanichakij et al., in prep) across the

³Data obtained from <https://dawn-cph.github.io/dja/v6> data release

following bands to calculate the total flux falling within the slit aperture: $F115W$, $F150W$, $F200W$, $F277W$, $F356W$, $F410M$, $F444W$.

To obtain our NIRSpec spectrophotometry we take advantage of the fact that by definition the *uniform* pathloss correction file is simply the inverse of the pathloss correction for a centered point source ([49], p.10). This arises because a uniform source has zero absolute pathloss. Thus by applying the uniform pathloss one simply gets the flux through the slit, regardless of image morphology. To achieve this we reduce all our spectroscopic data forcing the NIRSpec pipeline to assume them as point sources for calibration. We further remove the `pathloss` step in the stage 2 pipeline that would correct for de-centering. Then we optimally extract 1D spectra and correct these using the uniform pathloss reference file. At each dither position we approximated our sources to be illuminated following a 3-slitlet pattern, given currently there are no JWST reference files for a 5-slitlet slit. We predict the result of this process to agree closely with the PRIMER photometry.

In Figure 5 we show this comparison, both before and after uniform pathloss correction is applied for ZF-3651. This is an ideal test case as this is an extended galaxy that sits near the edge of its slit. It can be seen that after this correction the spectrum, and filter fluxes computed from the spectrum, agree well with the NIRC*am* pseudo-slit photometry ($RMS \sim 2.5 \times 10^{-21} \text{ erg/s/cm}^2/\text{\AA}$). Note this does not mean it represents the true flux on sky within the aperture because both NIRC*am* and NIRSpec data now include slit losses from PSF wings that will increase with wavelength. Any non-uniform source, even one with a uniform colour, will see a small chromatic shift due to the wavelength dependent PSF when viewed through a slit aperture. However the fact that NIRC*am* and NIRSpec agree means we have an understanding of the spectrophotometry of complex sources and validates our assumption that two instruments have very similar PSFs.

We next determine the correction to total spectrophotometry using the PRIMER photometry. First we investigate the degree of any spectral shift introduced by this by using the $F150W - F444W$ colour as a proxy (as it straddles the Balmer breaks in our objects). We find the median shift in colour between slit and total to be at the $\sim -0.04 \pm 0.02$ mag level which we attribute to the relatively homogeneous colours of the quiescent galaxies.

We then used the photometry computed using the spectra to derive an empirical polynomial calibration function to match the total photometric magnitude of the objects. For this purpose we use all PRIMER photometry with a $S/N > 20$. We fit a 2nd order polynomial to the line flux difference and apply that correction to the observed uniform pathloss corrected spectra. Similar to before, we further validate that this process does not introduce an extra color bias to the spectra. We find the offset to be at the $\sim 0.01 \pm 0.08$ mag level. This scaled spectra is then used in spectral fitting using FAST++.

2.2 Spectrophotometric Fitting with FAST++

The galaxies studied in this work were selected from S18 for spectroscopic confirmation, and our FAST++ analysis closely mirrors the SFH analysis of S18. However, we allow the stellar metallicity to vary between 20-100% Z_{\odot} and make minor adjustments to step sizes of the parameters that define the SFH as outlined in Table 2.

S18 tailored the analytical form of the SFH to specifically suite quiescent galaxies at $z \sim 3 - 4$. The elaborate functional form developed by S18 allows the star-forming phase of the galaxies to be broken into two separate epochs. The primary phase of the SFH comprise of an exponentially increasing and decreasing window. Additionally, a scaling factor is introduced during the last 10-300 Myr of the galaxy SFH to momentarily increase the SFH near the observation time. This adjustment is crucial for accounting for recent SFHs in otherwise quenched galaxies, especially when considering star formation rate (SFR) measurements derived from FIR observations. We refer the readers to [3, 14] for further information.

NIRSpec PRISM mode has a non-linear spectral resolution and dispersion. Thus, for accurate spectral fitting we need to convolve the model spectra with an accurate dispersion based on the source profile on the slit. We use the $1 - 5\mu\text{m}$ NIRC*am* images from PRIMER to compute an empirical function on how the FWHM of the source image vary on the slit as a function of wavelength. This is well approximated by a linear function for our sources. We then multiply this function by the PRISM dispersion provided by STScI⁴ (also [10]) to obtain the LSF of the galaxies. This is then used by FAST++ to convolve the model spectra to match with the observations. The spectral resolution computed for our sources are shown by Figure 6 and more details are presented in [11].

Table 2 The SFH parameters used in FAST++.

Free Parameter	Lower Bound	Upper Bound	Step Size
t_{burst} (Gyr)	0.01	tH(z)	0.025 dex
τ_{rise} (Gyr)	0.01	3	0.25 dex
τ_{decl} (Gyr)	0.01	3	0.05 dex
R_{SFR}	10^{-2}	10^5	0.1 dex
t_{free} (Myr)	10	300	0.25 dex

Acknowledgments. This work is based on observations made with the NASA/ESA/CSA James Webb Space Telescope. The data were obtained from the Mikulski Archive for Space Telescopes at the Space Telescope Science Institute, which is operated by the Association of Universities for Research in Astronomy, Inc., under NASA contract NAS 5-03127 for JWST. These observations are associated with program 2565. We thank all the hard work of the JWST team which made this great observatory possible. We thank

⁴<https://jwst-docs.stsci.edu/jwst-near-infrared-spectrograph/nirspec-instrumentation/nirspec-dispersers-and-filters#NIRSpecDispersersandFilters-DispersioncurvesfortheNIRSpecdispersers>

Michael Maseda and Allison Strom for helpful discussions during the data reduction process. T.N., K. G., and C.J. acknowledge support from Australian Research Council Laureate Fellowship FL180100060. This work has benefited from funding from the Australian Research Council Centre of Excellence for All Sky Astrophysics in 3 Dimensions (ASTRO 3D), through project number CE170100013. The Cosmic Dawn Center is funded by the Danish National Research Foundation (DNRF) under grant DNRF140. P.O. is supported by the Swiss National Science Foundation through project grant 200020_207349. This work received funding from the Swiss State Secretariat for Education, Research and Innovation (SERI).

Data Availability. Data used in the analysis will be made public upon acceptance of the manuscript.

Code Availability. All softwares used in this analysis are publicly available. Relevant codes used in making figures will be made public upon acceptance of the manuscript.

References

- [1] Glazebrook, K., Schreiber, C., Labbé, I., Nanayakkara, T., Kacprzak, G.G., Oesch, P.A., Papovich, C., Spitler, L.R., Straatman, C.M.S., Tran, K.-V.H., Yuan, T.: A massive, quiescent galaxy at a redshift of 3.717. *Nature* **544**, 71–74 (2017) <https://arxiv.org/abs/1702.01751> [astro-ph.GA]. <https://doi.org/10.1038/nature21680>
- [2] Marsan, Z.C., Marchesini, D., Brammer, G.B., Geier, S., Kado-Fong, E., Labbé, I., Muzzin, A., Stefanon, M.: A Spectroscopic Follow-up Program of Very Massive Galaxies at $3 \lesssim z \lesssim 4$: Confirmation of Spectroscopic Redshifts, and a High Fraction of Powerful AGNs. *ApJ* **842**(1), 21 (2017) <https://arxiv.org/abs/1606.05350> [astro-ph.GA]. <https://doi.org/10.3847/1538-4357/aa7206>
- [3] Schreiber, C., Labbé, I., Glazebrook, K., Bekiaris, G., Papovich, C., Costa, T., Elbaz, D., Kacprzak, G.G., Nanayakkara, T., Oesch, P.: Jekyll & Hyde: quiescence and extreme obscuration in a pair of massive galaxies 1.5 Gyr after the Big Bang. *A&A* **611**, 22 (2018) <https://arxiv.org/abs/1709.03505> [astro-ph.GA]. <https://doi.org/10.1051/0004-6361/201731917>
- [4] Tanaka, M., Valentino, F., Toft, S., Onodera, M., Shimakawa, R., Ceverino, D., Faisst, A.L., Gallazzi, A., Gómez-Guijarro, C., Kubo, M., Magdis, G.E., Steinhardt, C.L., Stockmann, M., Yabe, K., Zabl, J.: Stellar Velocity Dispersion of a Massive Quenching Galaxy at $z = 4.01$. *ApJ* **885**(2), 34 (2019) <https://arxiv.org/abs/1909.10721> [astro-ph.GA]. <https://doi.org/10.3847/2041-8213/ab4ff3>

- [5] Carnall, A.C., Walker, S., McLure, R.J., Dunlop, J.S., McLeod, D.J., Cullen, F., Wild, V., Amorin, R., Bolzonella, M., Castellano, M., Cimatti, A., Cucciati, O., Fontana, A., Gargiulo, A., Garilli, B., Jarvis, M.J., Pentericci, L., Pozzetti, L., Zamorani, G., Calabro, A., Hathi, N.P., Koekoemoer, A.M.: Timing the earliest quenching events with a robust sample of massive quiescent galaxies at $2 < z < 5$. *MNRAS* **496**(1), 695–707 (2020) <https://arxiv.org/abs/2001.11975> [astro-ph.GA]. <https://doi.org/10.1093/mnras/staa1535>
- [6] Forrest, B., Annunziatella, M., Wilson, G., Marchesini, D., Muzzin, A., Cooper, M.C., Marsan, Z.C., McConachie, I., Chan, J.C.C., Gomez, P., Kado-Fong, E., Barbera, F., Labbé, I., Lange-Vagle, D., Nantais, J., Nonino, M., Peña, T., Saracco, P., Stefanon, M., van der Burg, R.F.J.: An Extremely Massive Quiescent Galaxy at $z = 3.493$: Evidence of Insufficiently Rapid Quenching Mechanisms in Theoretical Models. *ApJ* **890**(1), 1 (2020) <https://arxiv.org/abs/1910.10158> [astro-ph.GA]. <https://doi.org/10.3847/2041-8213/ab5b9f>
- [7] Forrest, B., Marsan, Z.C., Annunziatella, M., Wilson, G., Muzzin, A., Marchesini, D., Cooper, M.C., Chan, J.C.C., McConachie, I., Gomez, P., Kado-Fong, E., Barbera, F.L., Lange-Vagle, D., Nantais, J., Nonino, M., Saracco, P., Stefanon, M., van der Burg, R.F.J.: The Massive Ancient Galaxies at $z < 3$ NEar-infrared (MAGAZ3NE) Survey: Confirmation of Extremely Rapid Star Formation and Quenching Timescales for Massive Galaxies in the Early Universe. *ApJ* **903**(1), 47 (2020) <https://arxiv.org/abs/2009.07281> [astro-ph.GA]. <https://doi.org/10.3847/1538-4357/abb819>
- [8] Valentino, F., Tanaka, M., Davidzon, I., Toft, S., Gómez-Guijarro, C., Stockmann, M., Onodera, M., Brammer, G., Ceverino, D., Faisst, A.L., Gallazzi, A., Hayward, C.C., Ilbert, O., Kubo, M., Magdis, G.E., Selsing, J., Shimakawa, R., Sparre, M., Steinhardt, C., Yabe, K., Zabl, J.: Quiescent Galaxies 1.5 Billion Years after the Big Bang and Their Progenitors. *ApJ* **889**(2), 93 (2020) <https://arxiv.org/abs/1909.10540> [astro-ph.GA]. <https://doi.org/10.3847/1538-4357/ab64dc>
- [9] Merlin, E., Fortuni, F., Torelli, M., Santini, P., Castellano, M., Fontana, A., Grazian, A., Pentericci, L., Pilo, S., Schmidt, K.B.: Red and dead CANDELS: massive passive galaxies at the dawn of the Universe. *MNRAS* **490**(3), 3309–3328 (2019) <https://arxiv.org/abs/1909.07996> [astro-ph.GA]. <https://doi.org/10.1093/mnras/stz2615>
- [10] Jakobsen, P., Ferruit, P., Alves de Oliveira, C., Arribas, S., Bagnasco, G., Barho, R., Beck, T.L., Birkmann, S., Böker, T., Bunker, A.J., Charlot, S., de Jong, P., de Marchi, G., Ehrenwinkler, R., Falcolini, M., Fels, R., Franx, M., Franz, D., Funke, M., Giardino, G., Gnata, X., Holota, W.,

- Honnen, K., Jensen, P.L., Jentsch, M., Johnson, T., Jollet, D., Karl, H., Kling, G., Köhler, J., Kolm, M.-G., Kumari, N., Lander, M.E., Lemke, R., López-Caniego, M., Lützgendorf, N., Maiolino, R., Manjavacas, E., Marston, A., Maschmann, M., Maurer, R., Messerschmidt, B., Moseley, S.H., Mosner, P., Mott, D.B., Muzerolle, J., Pirzkal, N., Pittet, J.-F., Plitzke, A., Posselt, W., Rapp, B., Rauscher, B.J., Rawle, T., Rix, H.-W., Rödel, A., Rumler, P., Sabbi, E., Salvignol, J.-C., Schmid, T., Sirianni, M., Smith, C., Strada, P., te Plate, M., Valenti, J., Wettemann, T., Wiehe, T., Wiesmayer, M., Willott, C.J., Wright, R., Zeidler, P., Zincke, C.: The Near-Infrared Spectrograph (NIRSpec) on the James Webb Space Telescope. I. Overview of the instrument and its capabilities. *A&A* **661**, 80 (2022) <https://arxiv.org/abs/2202.03305> [astro-ph.IM]. <https://doi.org/10.1051/0004-6361/202142663>
- [11] Glazebrook, K., Nanayakkara, T., Schreiber, C., Lagos, C., Kawinwanichakij, L., Jacobs, C., Chittenden, H., Brammer, G., Kacprzak, G.G., Labbe, I., Marchesini, D., Marsan, Z.C., Oesch, P.A., Papovich, C., Remus, R.-S., Tran, K.-V.H., Esdaile, J., Chandro Gomez, A.: An extraordinarily massive galaxy that formed its stars at *z*_{rsim}11. arXiv e-prints, 2308–05606 (2023) <https://arxiv.org/abs/2308.05606> [astro-ph.GA]. <https://doi.org/10.48550/arXiv.2308.05606>
- [12] Behroozi, P., Silk, J.: The most massive galaxies and black holes allowed by Λ CDM. *MNRAS* **477**(4), 5382–5387 (2018) <https://arxiv.org/abs/1609.04402> [astro-ph.GA]. <https://doi.org/10.1093/mnras/sty945>
- [13] Remus, R.-S., Dolag, K., Dannerbauer, H.: The Young and the Wild: What happens to Protoclusters forming at $z = 4$? arXiv e-prints, 2208–01053 (2022) <https://arxiv.org/abs/2208.01053> [astro-ph.CO]
- [14] Schreiber, C., Glazebrook, K., Nanayakkara, T., Kacprzak, G.G., Labbé, I., Oesch, P., Yuan, T., Tran, K.-V., Papovich, C., Spitler, L., Straatman, C.: Near infrared spectroscopy and star-formation histories of $3 \leq z \leq 4$ quiescent galaxies. *A&A* **618**, 85 (2018) <https://arxiv.org/abs/1807.02523> [astro-ph.GA]. <https://doi.org/10.1051/0004-6361/201833070>
- [15] Williams, R.J., Quadri, R.F., Franx, M., van Dokkum, P., Labbé, I.: Detection of Quiescent Galaxies in a Bicolor Sequence from $Z = 0 - 2$. *ApJ* **691**, 1879–1895 (2009) <https://arxiv.org/abs/0806.0625>. <https://doi.org/10.1088/0004-637X/691/2/1879>
- [16] McLean, I.S., Steidel, C.C., Matthews, K., Epps, H., Adkins, S.M.: MOS-FIRE: a multi-object near-infrared spectrograph and imager for the Keck Observatory. In: Society of Photo-Optical Instrumentation Engineers (SPIE) Conference Series. Society of Photo-Optical Instrumentation Engineers (SPIE) Conference Series, vol. 7014 (2008). <https://doi.org/10.1117/12.7014>

[1117/12.788142](https://doi.org/10.1117/12.788142)

- [17] Rawle, T.D., Giardino, G., Franz, D.E., Rapp, R., te Plate, M., Zincke, C.A., Abul-Huda, Y.M., Alves de Oliveira, C., Bechtold, K., Beck, T., Birkmann, S.M., Böker, T., Ehrenwinkler, R., Ferruit, P., Garland, D., Jakobsen, P., Karakla, D., Karl, H., Keyes, C.D., Koehler, R., Nimisha, K., Lützgendorf, N., Manjavacas, E., Marston, A., Moseley, S.H., Mosner, P., Muzerolle, J., Ogle, P., Proffitt, C., Sabbi, E., Sirianni, M., Wahlgren, G., Wislowski, E., Wright, R.H., Wu, C.R., Zeidler, P.: In-flight performance of the NIRSpec micro shutter array. In: Coyle, L.E., Matsuura, S., Perrin, M.D. (eds.) *Space Telescopes and Instrumentation 2022: Optical, Infrared, and Millimeter Wave*. Society of Photo-Optical Instrumentation Engineers (SPIE) Conference Series, vol. 12180, p. 121803 (2022). <https://doi.org/10.1117/12.2629231>
- [18] Straatman, C.M.S., Spitler, L.R., Quadri, R.F., Labbé, I., Glazebrook, K., Persson, S.E., Papovich, C., Tran, K.-V.H., Brammer, G.B., Cowley, M., Tomczak, A., Nanayakkara, T., Alcorn, L., Allen, R., Broussard, A., van Dokkum, P., Forrest, B., van Houdt, J., Kacprzak, G.G., Kawinwanichakij, L., Kelson, D.D., Lee, J., McCarthy, P.J., Mehtens, N., Monson, A., Murphy, D., Rees, G., Tilvi, V., Whitaker, K.E.: The FourStar Galaxy Evolution Survey (ZFOURGE): Ultraviolet to Far- infrared Catalogs, Medium-bandwidth Photometric Redshifts with Improved Accuracy, Stellar Masses, and Confirmation of Quiescent Galaxies to $z \sim 3.5$. *ApJ* **830**, 51 (2016) [astro-ph.GA]. <https://doi.org/10.3847/0004-637X/830/1/51>
- [19] Bushouse, H., Eisenhamer, J., Dencheva, N., Davies, J., Greenfield, P., Morrison, J., Hodge, P., Simon, B., Grumm, D., Droettboom, M., Slavich, E., Sosey, M., Pauly, T., Miller, T., Jedrzejewski, R., Hack, W., Davis, D., Crawford, S., Law, D., Gordon, K., Regan, M., Cara, M., MacDonald, K., Bradley, L., Shanahan, C., Jamieson, W.: JWST Calibration Pipeline. Zenodo (2022). <https://doi.org/10.5281/zenodo.7038885>
- [20] Poggianti, B.M., Barbaro, G.: Indicators of star formation: 4000 Å break and Balmer lines. *A&A* **325**, 1025–1030 (1997) <https://arxiv.org/abs/astro-ph/9703067> [astro-ph]
- [21] Binggeli, C., Zackrisson, E., Ma, X., Inoue, A.K., Vikaeus, A., Hashimoto, T., Mawatari, K., Shimizu, I., Ceverino, D.: Balmer breaks in simulated galaxies at $z \lesssim 6$. *MNRAS* **489**(3), 3827–3835 (2019) <https://arxiv.org/abs/1908.11393> [astro-ph.GA]. <https://doi.org/10.1093/mnras/stz2387>
- [22] Juneau, S., Bournaud, F., Charlot, S., Daddi, E., Elbaz, D., Trump, J.R., Brinchmann, J., Dickinson, M., Duc, P.-A., Gobat, R., Jean-Baptiste, I., Le Floc'h, É., Lehnert, M.D., Pacifici, C., Pannella, M., Schreiber,

- C.: Active Galactic Nuclei Emission Line Diagnostics and the Mass-Metallicity Relation up to Redshift $z \sim 2$: The Impact of Selection Effects and Evolution. *ApJ* **788**(1), 88 (2014) <https://arxiv.org/abs/1403.6832> [astro-ph.GA]. <https://doi.org/10.1088/0004-637X/788/1/88>
- [23] Antwi-Danso, J., Papovich, C., Leja, J., Marchesini, D., Marsan, Z.C., Martis, N.S., Labbé, I., Muzzin, A., Glazebrook, K., Straatman, C.M.S., Tran, K.-V.H.: Beyond UVJ: Color Selection of Galaxies in the JWST Era. arXiv e-prints, 2207–07170 (2022) <https://arxiv.org/abs/2207.07170> [astro-ph.GA]
- [24] McLean, I.S., Steidel, C.C., Epps, H.W., Konidaris, N., Matthews, K.Y., Adkins, S., Aliado, T., Brims, G., Canfield, J.M., Cromer, J.L., Fucik, J., Kulas, K., Mace, G., Magnone, K., Rodriguez, H., Rudie, G., Trainor, R., Wang, E., Weber, B., Weiss, J.: MOSFIRE the multi-object spectrometer for infra-red exploration at the Keck Observatory. In: McLean, I.S., Ramsay, S.K., Takami, H. (eds.) *Ground-based and Airborne Instrumentation for Astronomy IV*, vol. 8446, pp. 84460–8446015. SPIE-Intl Soc Optical Eng, ??? (2012). <https://doi.org/10.1117/12.924794>. <http://dx.doi.org/10.1117/12.924794>
- [25] Bruzual A., G.: Spectral evolution of galaxies. I. Early-type systems. *ApJ* **273**, 105–127 (1983). <https://doi.org/10.1086/161352>
- [26] Bruzual, G., Charlot, S.: Stellar population synthesis at the resolution of 2003. *MNRAS* **344**, 1000–1028 (2003) <https://arxiv.org/abs/astro-ph/0309134>. <https://doi.org/10.1046/j.1365-8711.2003.06897.x>
- [27] Chabrier, G.: Galactic stellar and substellar initial mass function. *Publications of the Astronomical Society of the Pacific* **115**(809), 763–795 (2003)
- [28] Calzetti, D., Armus, L., Bohlin, R.C., Kinney, A.L., Koornneef, J., Storchi-Bergmann, T.: The Dust Content and Opacity of Actively Star-forming Galaxies. *ApJ* **533**, 682–695 (2000) <https://arxiv.org/abs/astro-ph/9911459>. <https://doi.org/10.1086/308692>
- [29] Tomczak, A.R., Quadri, R.F., Tran, K.-V.H., Labbé, I., Straatman, C.M.S., Papovich, C., Glazebrook, K., Allen, R., Brammer, G.B., Kacprzak, G.G., Kawinwanichakij, L., Kelson, D.D., McCarthy, P.J., Mehtens, N., Monson, A.J., Persson, S.E., Spitler, L.R., Tilvi, V., van Dokkum, P.: Galaxy Stellar Mass Functions from ZFOURGE/CANDELS: An Excess of Low-mass Galaxies since $z = 2$ and the Rapid Buildup of Quiescent Galaxies. *ApJ* **783**, 85 (2014) <https://arxiv.org/abs/1309.5972>. <https://doi.org/10.1088/0004-637X/783/2/85>
- [30] Valentino, F., Brammer, G., Gould, K.M.L., Kokorev, V., Fujimoto, S.,

- Kragh Jespersen, C., Vijayan, A.P., Weaver, J.R., Ito, K., Tanaka, M., Ilbert, O., Magdis, G.E., Whitaker, K.E., Faisst, A.L., Gallazzi, A., Gillman, S., Gimenez-Arteaga, C., Gomez-Guijarro, C., Kubo, M., Heintz, K.E., Hirschmann, M., Oesch, P., Onodera, M., Rizzo, F., Lee, M., Strait, V., Toft, S.: An Atlas of Color-selected Quiescent Galaxies at $z > 3$ in Public JWST Fields. arXiv e-prints, 2302–10936 (2023) <https://arxiv.org/abs/2302.10936> [astro-ph.GA]. <https://doi.org/10.48550/arXiv.2302.10936>
- [31] Long, A.S., Casey, C.M., Lagos, C.d.P., Lambrides, E.L., Zavala, J.A., Champagne, J., Cooper, O.R., Cooray, A.R.: Missing Giants: Predictions on Dust-Obscured Galaxy Stellar Mass Assembly Throughout Cosmic Time. arXiv e-prints, 2211–02072 (2022) <https://arxiv.org/abs/2211.02072> [astro-ph.GA]
- [32] Lustig, P., Strazzullo, V., Remus, R.-S., D’Eugenio, C., Daddi, E., Burkert, A., De Lucia, G., Delvecchio, I., Dolag, K., Fontanot, F., Gobat, R., Mohr, J.J., Onodera, M., Pannella, M., Pillepich, A.: Massive quiescent galaxies at $z \sim 3$: A comparison of selection, stellar population, and structural properties with simulation predictions. MNRAS **518**(4), 5953–5975 (2023) <https://arxiv.org/abs/2201.09068> [astro-ph.GA]. <https://doi.org/10.1093/mnras/stac3450>
- [33] D’Eugenio, C., Daddi, E., Gobat, R., Strazzullo, V., Lustig, P., Delvecchio, I., Jin, S., Cimatti, A., Onodera, M.: HST grism spectroscopy of $z \sim 3$ massive quiescent galaxies. Approaching the metamorphosis. A&A **653**, 32 (2021) <https://arxiv.org/abs/2012.02767> [astro-ph.GA]. <https://doi.org/10.1051/0004-6361/202040067>
- [34] Kalita, B.S., Daddi, E., D’Eugenio, C., Valentino, F., Rich, R.M., Gómez-Guijarro, C., Coogan, R.T., Delvecchio, I., Elbaz, D., Neill, J.D., Puglisi, A., Strazzullo, V.: An Ancient Massive Quiescent Galaxy Found in a Gas-rich $z \sim 3$ Group. ApJ **917**(2), 17 (2021) <https://arxiv.org/abs/2107.13241> [astro-ph.GA]. <https://doi.org/10.3847/2041-8213/ac16dc>
- [35] Carnall, A.C., McLeod, D.J., McLure, R.J., Dunlop, J.S., Begley, R., Cullen, F., Donnan, C.T., Hamadouche, M.L., Jewell, S.M., Jones, E.W., Pollock, C.L., Wild, V.: A surprising abundance of massive quiescent galaxies at $3 < z < 5$ in the first data from JWST CEERS. MNRAS **520**(3), 3974–3985 (2023) <https://arxiv.org/abs/2208.00986> [astro-ph.GA]. <https://doi.org/10.1093/mnras/stad369>
- [36] Valentini, M., Dolag, K., Borgani, S., Murante, G., Maio, U., Tornatore, L., Granato, G.L., Ragone-Figueroa, C., Burkert, A., Ragagnin, A., Rasia, E.: Impact of H₂-driven star formation and stellar feedback

- from low-enrichment environments on the formation of spiral galaxies. *MNRAS* **518**(1), 1128–1147 (2023) <https://arxiv.org/abs/2207.13710> [astro-ph.GA]. <https://doi.org/10.1093/mnras/stac2110>
- [37] Carnall, A.C., McLure, R.J., Dunlop, J.S., McLeod, D.J., Wild, V., Cullen, F., Magee, D., Begley, R., Cimatti, A., Donnan, C.T., Hamadouche, M.L., Jewell, S.M., Walker, S.: A massive quiescent galaxy at redshift 4.658. arXiv e-prints, 2301–11413 (2023) <https://arxiv.org/abs/2301.11413> [astro-ph.GA]. <https://doi.org/10.48550/arXiv.2301.11413>
- [38] Maiolino, R., Scholtz, J., Witstok, J., Carniani, S., D’Eugenio, F., de Graaff, A., Uebler, H., Tacchella, S., Curtis-Lake, E., Arribas, S., Bunker, A., Charlot, S., Chevallard, J., Curti, M., Looser, T.J., Maseda, M.V., Rawle, T., Rodriguez Del Pino, B., Willott, C.J., Egami, E., Eisenstein, D., Hainline, K., Robertson, B., Williams, C.C., Willmer, C.N.A., Baker, W.M., Boyett, K., DeCoursey, C., Fabian, A.C., Helton, J.M., Ji, Z., Jones, G.C., Kumari, N., Laporte, N., Nelson, E., Perna, M., Sandles, L., Shivaei, I., Sun, F.: A small and vigorous black hole in the early Universe. arXiv e-prints, 2305–12492 (2023) <https://arxiv.org/abs/2305.12492> [astro-ph.GA]. <https://doi.org/10.48550/arXiv.2305.12492>
- [39] Looser, T.J., D’Eugenio, F., Maiolino, R., Witstok, J., Sandles, L., Curtis-Lake, E., Chevallard, J., Tacchella, S., Johnson, B.D., Baker, W.M., Suess, K.A., Carniani, S., Ferruit, P., Arribas, S., Bonaventura, N., Bunker, A.J., Cameron, A.J., Charlot, S., Curti, M., de Graaff, A., Maseda, M.V., Rawle, T., Rix, H.-W., Rodriguez Del Pino, B., Smit, R., Übler, H., Willott, C., Alberts, S., Egami, E., Eisenstein, D.J., Endsley, R., Hausen, R., Rieke, M., Robertson, B., Shivaei, I., Williams, C.C., Boyett, K., Chen, Z., Ji, Z., Jones, G.J., Kumari, N., Nelson, E., Perna, M., Saxena, A., Scholtz, J.: Discovery of a quiescent galaxy at $z=7.3$. arXiv e-prints, 2302–14155 (2023) <https://arxiv.org/abs/2302.14155> [astro-ph.GA]. <https://doi.org/10.48550/arXiv.2302.14155>
- [40] Strait, V., Brammer, G., Muzzin, A., Dezprez, G., Asada, Y., Abraham, R., Bradač, M., Iyer, K.G., Martis, N., Mowla, L., Noirot, G., Sarrouh, G., Sawicki, M., Willott, C., Gould, K., Grindlay, T., Matharu, J., Rihtaršič, G.: An extremely compact, low-mass post-starburst galaxy at $z = 5.2$. arXiv e-prints, 2303–11349 (2023) <https://arxiv.org/abs/2303.11349> [astro-ph.GA]. <https://doi.org/10.48550/arXiv.2303.11349>
- [41] Schaye, J., Kugel, R., Schaller, M., Helly, J.C., Braspenning, J., Elbers, W., McCarthy, I.G., van Daalen, M.P., Vandenbroucke, B., Frenk, C.S., Kwan, J., Salcido, J., Bahé, Y.M., Borrow, J., Chaikin, E., Hahn, O., Huško, F., Jenkins, A., Lacey, C.G., Nobels, F.S.J.: The

- FLAMINGO project: cosmological hydrodynamical simulations for large-scale structure and galaxy cluster surveys. arXiv e-prints, 2306–04024 (2023) <https://arxiv.org/abs/2306.04024> [astro-ph.CO]. <https://doi.org/10.48550/arXiv.2306.04024>
- [42] Esdaile, J., Glazebrook, K., Labbé, I., Taylor, E., Schreiber, C., Nanayakkara, T., Kacprzak, G.G., Oesch, P.A., Tran, K.-V.H., Papovich, C., Spitler, L., Straatman, C.M.S.: Consistent Dynamical and Stellar Masses with Potential Light IMF in Massive Quiescent Galaxies at $3 < z < 4$ Using Velocity Dispersions Measurements with MOSFIRE. *ApJ* **908**(2), 35 (2021) <https://arxiv.org/abs/2010.09738> [astro-ph.GA]. <https://doi.org/10.3847/2041-8213/ab111e>
- [43] Nanayakkara, T., Esdaile, J., Glazebrook, K., Espejo Salcedo, J.M., Durre, M., Jacobs, C.: Massive High-Redshift Quiescent Galaxies With JWST. arXiv e-prints, 2103–01459 (2021) <https://arxiv.org/abs/2103.01459> [astro-ph.GA]
- [44] Kalita, B.S., Daddi, E., Bournaud, F., Rich, R.M., Valentino, F., Gómez-Guijarro, C., Codis, S., Delvecchio, I., Elbaz, D., Strazzullo, V., de Souza Magalhaes, V., Pety, J., Tan, Q.: Bulge formation inside quiescent lopsided stellar disks: Connecting accretion, star formation, and morphological transformation in a $z \sim 3$ galaxy group. *A&A* **666**, 44 (2022) <https://arxiv.org/abs/2206.05217> [astro-ph.GA]. <https://doi.org/10.1051/0004-6361/202243100>
- [45] Chandar, R., Caputo, M., Linden, S., Mok, A., Whitmore, B.C., Calzetti, D., Elmegreen, D.M., Lee, J.C., Ubeda, L., White, R., Cook, D.O.: Arp 220: A Post-starburst Galaxy with Little Current Star Formation outside of Its Nuclear Disks. *ApJ* **943**(2), 142 (2023) <https://arxiv.org/abs/2301.07180> [astro-ph.GA]. <https://doi.org/10.3847/1538-4357/acac96>
- [46] Chevallard, J., Charlot, S.: Modelling and interpreting spectral energy distributions of galaxies with BEAGLE. *MNRAS* **462**, 1415–1443 (2016) <https://arxiv.org/abs/1603.03037>. <https://doi.org/10.1093/mnras/stw1756>
- [47] Johnson, B.D., Leja, J., Conroy, C., Speagle, J.S.: Stellar Population Inference with Prospector. *ApJS* **254**(2), 22 (2021) <https://arxiv.org/abs/2012.01426> [astro-ph.GA]. <https://doi.org/10.3847/1538-4365/abef67>
- [48] Horne, K.: An optimal extraction algorithm for CCD spectroscopy. *PASP* **98**, 609–617 (1986). <https://doi.org/10.1086/131801>
- [49] Ferruit, P.: The correction of path losses for uniform and point sources. ESA NIRSPEC Technical Note 'ESA-JWST-SCI-NRS-TN-2016-017' (2016). https://dms.cosmos.esa.int/COSMOS/doc_fetch.php?

[id=3520285](#) [Accessed: 20/Jul/2023]

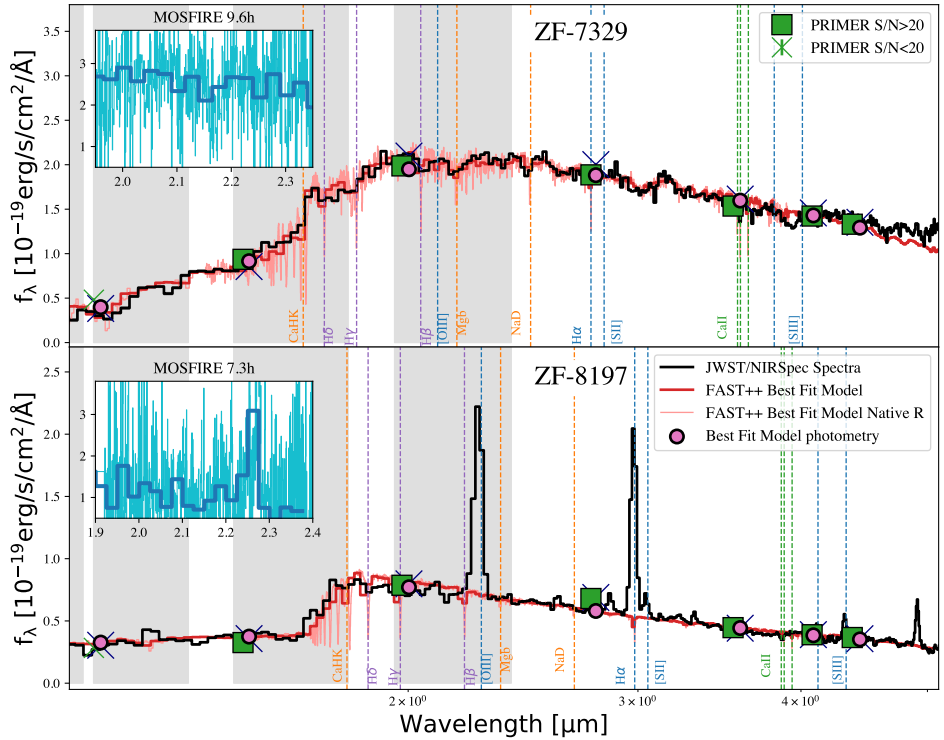


Fig. 2 The **top** and **bottom** panels present JWST/NIRSpec spectra of two quiescent galaxy candidates, ZF-7329 and ZF-8197 respectively, observed over the ZFOURGE-UDS field. ZF-7329 is one of the oldest known quiescent galaxies in the $z > 3$ Universe [11]. ZF-8197 is a quiescent galaxy in our sample that exhibits strong [O III] λ 5007 and H α EWs, possibly driven by an AGN. The spectra were optimally extracted [48] and flux-calibrated using PRIMER photometry. Grey bands highlight the KECK/MOSFIRE Y, J, H, K bands (from left to right). To improve clarity, spectra are trimmed at $< 1.1 \mu\text{m}$. For each galaxy, we also display the PRIMER total photometry in two bins based on the S/N. The best-fit FAST++ template and the best-fit model photometry for the observed filters used in FAST++ are shown in the panels. Commonly observed rest-frame emission and absorption features are marked in the spectra. Inset in each panel display the ground-based K-band MOSFIRE spectra presented in S18. The thin cyan lines represent the MOSFIRE spectra at its native resolution of $R \sim 3000$, while the thick blue lines correspond to the MOSFIRE spectra at a resolution similar to that of the JWST/NIRSpec PRISM observations at $\lambda_{\text{obs}} \sim 2 \mu\text{m}$ ($R \sim 100$). In S18, we managed to achieve spectroscopic confirmation for ZF-8197, thanks to its strong [O III] λ 5007 emission line falling within the K band. However, due to the absence of prominent emission/absorption lines and limited wavelength coverage on the ground for capturing the spectral shape at $\sim 4000 \text{\AA}$, we were unable to confirm ZF-7329 spectroscopically, even with $\sim 10\text{h}$ of Keck/MOSFIRE exposure time.

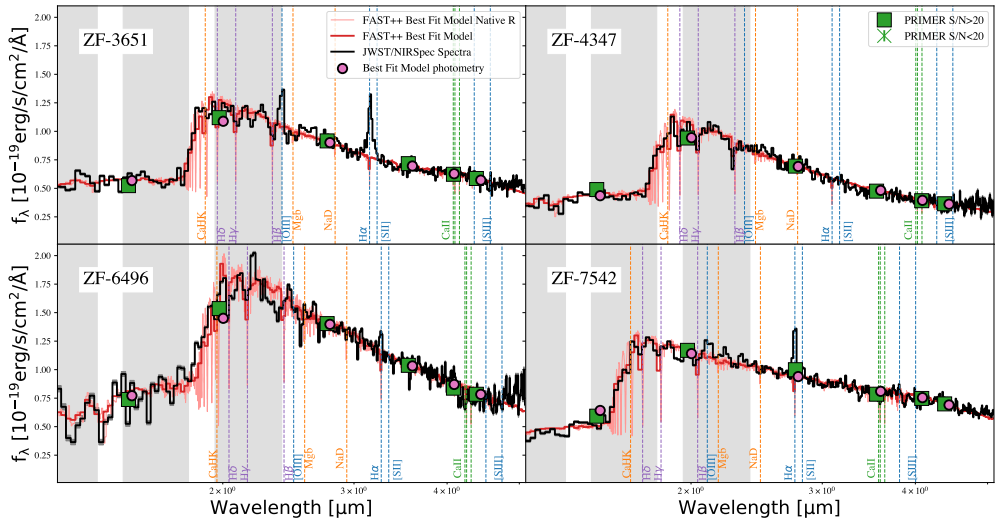


Fig. 3 JWST/NIRSpec spectra of the remaining four quiescent galaxy candidates, ZF-3651, ZF-4347, ZF-6496, and ZF-7542, obtained from the ZFOURGE-UDS field. The format of this figure mirrors that of Figure 2, with the exception of the MOSFIRE insets. The upper panels display the spectra of ZF-3651 and ZF-4347 (from left to right), while the lower panels show the spectra of ZF-6496 and ZF-7542.

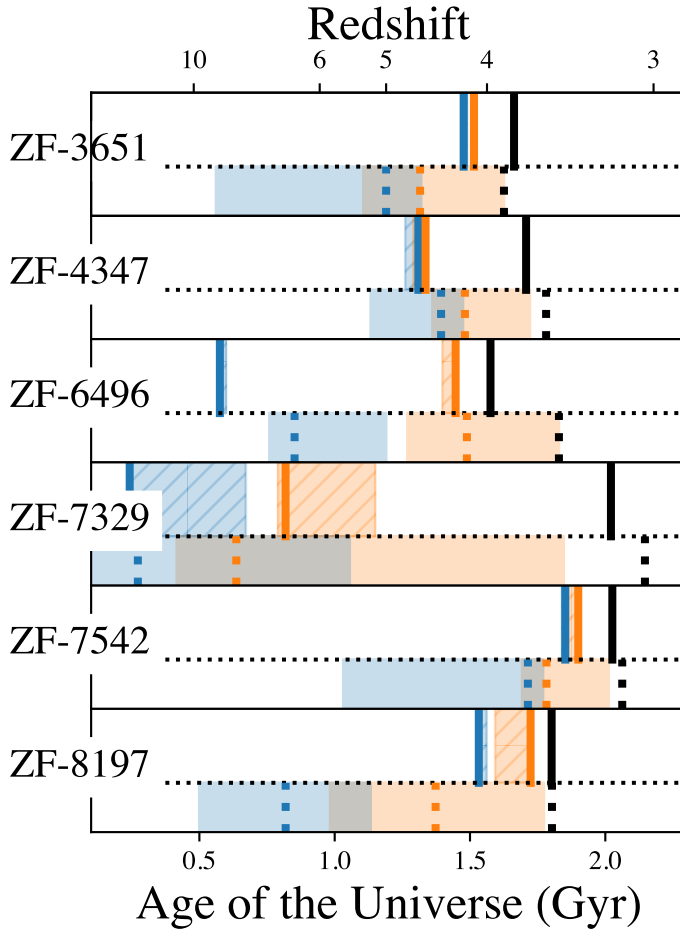


Fig. 4 The best-fit SFHs of our galaxies. The blue vertical lines indicate the time at which each galaxy formed 50% of its stellar mass, with the associated 3σ error parameterized by 100 MCMC iterations is depicted by the blue shaded region. We show the quenching time, as defined by S18 (the time at which the galaxy’s Star Formation Rate (SFR) falls below 10% of its primary SFR episode, as detailed in Section 4.1 of S18), by orange vertical lines. The associated error is shaded in orange. The black vertical line represents the age of the Universe when the galaxy is being observed. For each galaxy, the top panels depict the improved constraints acquired through our JWST/NIRSpec observations. The lower panels (below the dotted lines) present constraints reported in S18. For clarity, we use vertical dashed lines to represent the best-fit S18 values.

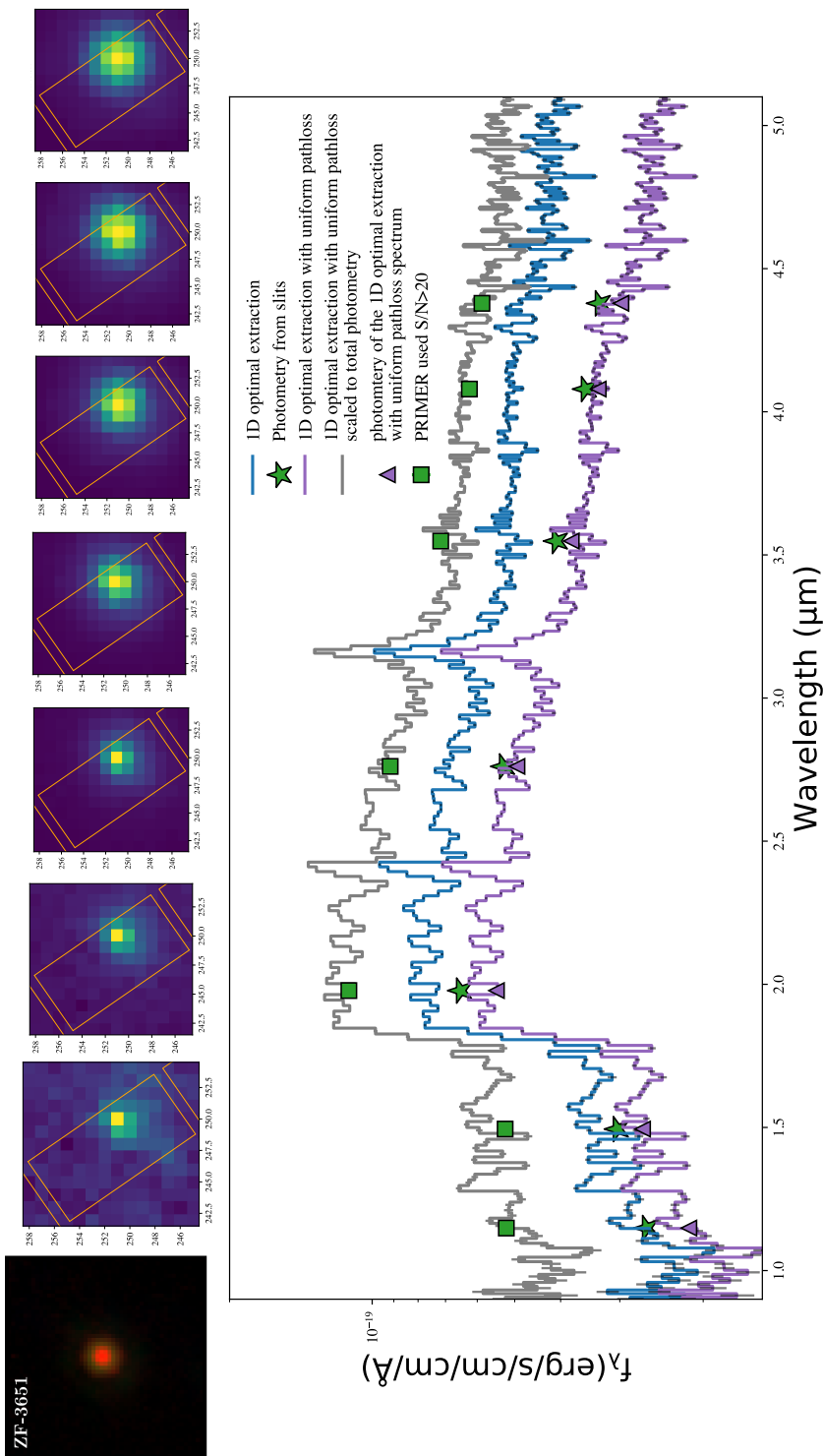


Fig. 5 An example demonstrating our total flux scaling process for ZF-3651. In the upper panel we show the NIRCams images of the galaxy. From left to right: $F115W$, $F200W$, and $F444W$ colour composite image covering rest frame optical bands. The next seven panels are the NIRCams $F115W$, $F150W$, $F200W$, $F277W$, $F356W$, $F410m$, and $F444W$ images. In each panel, the slit at dither position 1 is overlaid on the image. Flux through the slit is computed using the segmentation image of the source at all three dither positions. In the lower panel we show the 1D optimally extracted spectra of ZF-3651. In blue we show the 1D optimally extracted spectrum from the final 2D result from the JWST calibration pipeline. The spectrum after a uniform pathloss correction is applied is shown in purple. Photometry from the spectrum are shown by the purple triangles and the photometry computed through the slit images of the respective NIRCams bands are shown by the green stars. In grey we show the spectrum scaled to total NIRCams photometry (green squares).

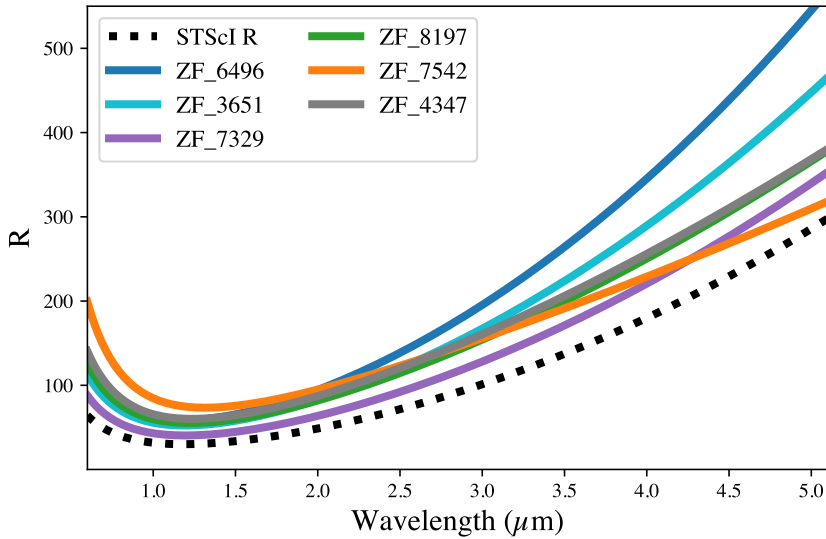


Fig. 6 The observed NIRSpect PRISM mode spectral resolution for our sample. These are empirically computed by modelling the image size on the NIRSpect MSA slit using PRIMER NIRCcam imaging. The spectral resolution of the NIRSpect PRISM mode for a uniformly illuminated slit is shown by the black dashed line for comparison. Given our objects do not fill the full slit width, the observed resolution is higher than the values presented by STScI.